Mendeleev Communications

Mendeleev Commun., 2027, **37**, in press

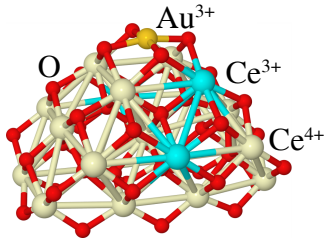
Bonding of Au_n (n = 1–4) gold species at the $Ce_{21}O_{42}$ ceria nanoparticle

Elena A. Ivanova-Shor,* Aleksey M. Shor, Svetlana S. Laletina and Vladimir A. Nasluzov

Institute of Chemistry and Chemical Technology, Siberian Branch of the Russian Academy of Sciences, 660036 Krasnoyarsk, Russian Federation. Fax: +7 391 249 4108; e-mail: eshor1977@gmail.com

DOI: 10.71267/mencom.8141

The active site of $Ce_{21}O_{42}$ ceria nanoparticles comprising four two-coordinated oxygen centers, an O_4 site, is adopted for the selective trapping of single gold atoms. Opposite to active sites of extended ceria surfaces, the O_4 site allows the formation of four Au–O bonds and the presence of gold not only in +1 but also in +3 oxidation states. Bonding of Au_n species with $n > 2$ at the O_4 site shows similar features with those anchored at extended CeO_2 surfaces.



Keywords: density functional theory, ceria nanoparticles, gold species, adsorption, oxidation state, coordination mode.

Ceria surfaces modified with single-atom and few-atom gold species are of interest due to their high applicability in catalysis for CO oxidation, CO_2 hydrogenation, and water–gas shift reaction.[1] The coordination modes, oxidation states, and binding energies of single and polyatomic gold species at stable nonpolar $CeO_2(111)$ surfaces were investigated theoretically.[2–4] The adsorbed gold atoms preferred the bridging O–Au–O adsorption mode with a moderate binding energy of about 1 eV. The adsorption of Au_n at polar $CeO_2(110)$ or $CeO_2(100)$ surfaces[5–8] was modeled less frequently despite the fact that they provided almost two times stronger metal–support binding and, therefore, reduced unwanted sintering of gold species. Moreover, nanostructured ceria surfaces (e.g., stepped surfaces that provided intersection of different ceria nanofacets) can be even more active and catalyze processes up to an order of magnitude faster compared to traditional 2D extended ceria surfaces.[9] This effect can be rationalized in view of the presence of low-coordinated and, hence, more mobile oxygen atoms, which can participate in oxidation processes.

Here, we report the density functional modeling of structural, electronic, and energetic features of gold species (single atom, dimer, trimer, and tetramer) adsorbed at active sites of ceria nanoparticles. As a ceria model, the stoichiometric $Ce_{21}O_{42}$ nanoparticle with an active center composed of four oxygen atoms of the $CeO_2(100)$ nanofacet, so-called O_4 pocket, has been used.[10] This model was elaborated as the smallest one in the series of ceria nanoparticles of enlarging sizes containing 21, 30, 40, and 80 cerium atoms.[11] The O_4 site of $Ce_{21}O_{42}$ and $Ce_{40}O_{80}$ was very effective in trapping single transition-metal atoms.[12,13] However, a systematic investigation of the anchoring of gold Au_n (n = 1, 2, 3,…) species of growing size at the O_4 pocket has not been performed as, for example, it was the case for $CeO_2(111)$, MgO(100), and graphite (0001) surfaces.[4] The present study is aimed at fulfilling this gap.

The calculations were carried out using the Vienna *ab initio* simulation package (VASP) code.[14] The computation parameters were taken as in our previous works.[13,15] The spin unrestricted eigenfunctions of the projector augmented wave method[16] were built for explicitly treated 11 valence electrons of each Au atom ($5s^14d^{10}$), 6 electrons of each O atom ($2s^22p^4$), and 12 electrons of each Ce atom ($5s^25p^66s^25d^14f^1$). For this purpose, the plane waves were included up to an energy cut-off of 415 eV.[17] The GGA+U scheme with the Perdew–Wang PW91 parametrization of the exchange-correlation functional and inclusion of the Hubbard-type on-site correction U-term of 4 eV for Ce 4*f* states was utilized. The Gaussian smearing of 0.05 eV was applied to the Kohn–Sham levels close to the Fermi energy, but the final energy values were extrapolated to zero smearing. The calculations of finite nanoclusters were performed at the Γ-point of the reciprocal space. To avoid interaction between repeated images of the nanoparticles, the vacuum gaps of ~1 nm in three Cartesian directions were utilized. The binding energies (E_b) of the Au_n species on the CeO_2 substrate were calculated as averaged values over n gold atoms: $E_b(Au_n/CeO_2) = [E(Au_n) + E(CeO_2) - E(Au_n/CeO_2)]/n$.

Figure 1 shows the lowest-energy structures of anchored Au_n (n = 1–4) moieties at ceria models. The geometries of all studied systems are collected in Table S2 of the Online Supplementary Materials. Given the preferred location of single gold atoms in the center of O_4 pockets previously modeled at $Ce_{40}O_{80}$ nanoparticles,[12] we used this geometry as a starting point. Three $Au_1/Ce_{21}O_{42}$ structures with similar gold binding energies within 0.2 eV were optimized (Table 1). The most stable model **1a** was characterized by four short Au–O contacts of 2.04–2.07 Å and gold atom lying 0.20–0.25 Å above the O_4-square plane (Figure 1). The Au center in structure **1a** had a charge of +0.91 e; the metal to support charge transfer was accompanied by the appearance of three reduced Ce^{3+} ions; that is, the gold center had the formal oxidation state +3. In two alternative structures **1b** and **1c** (Figure S2), Au atoms formed two short bonds of 2.06–2.07 Å and two long bonds of 2.74–2.79 Å with oxygen centers lying at the opposite sides of O_4 pockets and rose 0.35–0.85 Å above the O_4-square plane. Here, the charge of an Au center was +0.33 e, which is equivalent to the formal oxidation state +1 since the reduction of only one Ce^{3+} ion was observed. The adsorption energies of Au atoms in models **1a**, **1b**, and **1c** were 2.3, 2.2, and 2.1 eV, respectively. These values are smaller than E_b of 2.73 and 3.46 eV calculated for Au^+ and Au^{3+} ions at O_4 pockets of a larger $Ce_{40}O_{80}$ nanoparticle, respectively.[12]

© 2027 Mendeleev Communications

Note that the strengthening of metal–ceria bonding at O_4 sites by 0.3 eV with the growth of ceria nanoparticles from $Ce_{40}O_{80}$ to $Ce_{80}O_{160}$ has been previously reported for the Pd^{2+} ion.[12] The larger discrepancy in E_b for Au^{3+} can be explained by the larger electrostatic metal–support interaction. The PBE-calculated E_b values of 2.6–3.0 eV for Au^+ anchored at O–O bridge sites of the extended $CeO_2(100)$ surface were reported.[8] On the other hand, the values of 2.07, 2.11, and 2.19 eV[5] were obtained[5–7] for two-coordinated Au^+ adsorbed in a bridging mode at the $CeO_2(110)$ surface with Au–O bonds of 1.98 Å. Note that E_b of ~1.1–1.2 eV was calculated for the bridging adsorption of single Au atoms for nondefect $CeO_2(110)$[18] and $CeO_2(111)$[4,19,20] surfaces. Interestingly, the Au^+ ion coordinated at one O atom of the O_4 site had similarly small E_b of 1.03 eV (Table S2).

The most stable gold dimer in structure **2a** was preferably coordinated in slightly tilted vertical mode forming one Au–O bond of 2.07 Å in length. The Au–Au bond length of 2.52 Å was not changed upon adsorption with respect to a gas-phase digold molecule. The binding energy of Au_2 species in **2a** was 0.65 eV, which is slightly smaller than 1.03 eV for the adsorption of a single Au atom at the same O atom of the O_4 site.

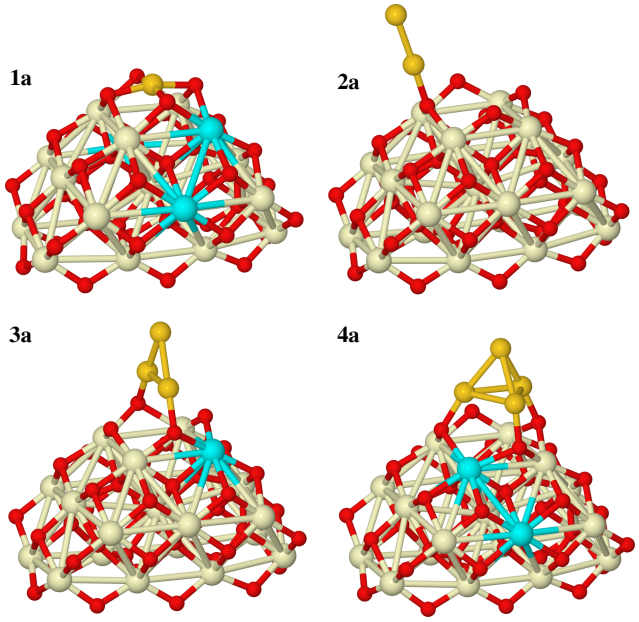


Figure 1 Optimized geometries of the most stable $Au_n/Ce_{21}O_{42}$ models (n = 1, 2, 3, and 4). The gold, oxygen, Ce^{4+}, and Ce^{3+} ions are colored yellow, red, beige, and blue, respectively.

Table 1 Parameters of Au_n species coordinated at the (100) nanofacet of $Ce_{21}O_{42}$ models: binding energy E_b, eV; Au–O and Au–Au distances, Å; Bader charge of the cluster $q(Au_n)$, e; and number of reduced Ce^{3+} ions $N(Ce^{3+})$. For the geometries of the models, see Figure 1 and Online Supplementary Materials.

Model	E_b	r(Au–O)	r(Au–Au)	$q(Au_n)$	$N(Ce^{3+})$
1a	2.30	2.04–2.07	–	0.90	3
1b	2.20	2.06, 2.07, 2.79	–	0.32	1
1c	2.10	2.06, 2.74, 2.77	–	0.33	1
2a	0.65	2.07	2.52	–0.17	0
2b	0.60	2.02, 2.07	2.87	0.54	2
2c	0.47	2.09, 2.13	2.58	0.25	1
3a	1.07	2.05, 2.06	2.61, 2.76	0.29	1
3b	1.05	2.06	2.61, 2.76	0.33	1
3c	0.29	2.06–2.10	2.85, 2.88	0.47	2
4a	0.66	2.03, 2.05	2.68–2.84	0.71	2
4b	0.67	2.04, 2.05	2.68–2.84	0.70	2
4c	0.51	2.06	2.60–2.84	0.27	1
4d	0.38	2.09–2.15	2.71, 2.73	0.48	2

Similar values of 1.0–1.2 eV were calculated for Au_2 adsorption at $CeO_2(110)$[18] and $CeO_2(111)$[4] while larger values of 1.75 and 2.0 eV were reported for the $Au_2/CeO_2(111)$ system.[3,20] Teng et al.[3] and Ghosh et al.[20] obtained two times larger E_b values due to the use of the different formula $E_b(Au_n/CeO_2) = [nE(Au) + E(CeO_2) – E(Au_n/CeO_2)]/n$, where the sum of the energies of single Au atoms nE(Au) was applied instead of the cluster energy $E(Au_n)$. In line with a study of Engel et al.,[4] the vertical model **2a** featured no charge transfer and oxidation of Au_2 moieties and, consequently, no appearance of reduced Ce^{3+} ions. The total charge of an Au_2 moiety was –0.17e with a positively charged Au atom (0.1e) in contact with the ceria oxygen center. Less stable model **2b** (E_b = 0.60 eV) with one Au atom of Au_2 located in the center of an O_4 pocket and the other one interacting with an O atom of the O_4 site featured a significantly elongated Au–Au distance of 2.87 Å, accompanied by reduction of two Ce^{4+} ions and oxidation of the Au_2 moiety (+0.54e). Structure **2c** with a nearly parallel orientation of the Au_2 moiety forming two nearly equal Au–O contacts of 2.09 and 2.13 Å and an Au–Au bond stretched to 2.58 Å was the least stable (E_b = 0.47 eV). Structure **2c** had one reduced Ce^{3+} ion and an Au_2 moiety with a total charge of +0.25e, which indicated the charge transfer and oxidation of the Au_2 moiety. All gold atoms of structures **2b** and **2c** were positively charged with a larger charge at the Au atom closer to the ceria surface.

Gold trimers were preferably adsorbed as triangles in a vertical position, forming two Au–O bonds of 2.06 Å. Two possible vertical adsorption modes **3a** and **3b** had binding energies of 1.07 and 1.05 eV, respectively. Preference of a vertical orientation of the Au_3 moiety at extended $CeO_2(111)$, (110), and (100) surfaces with E_b of 1.02, 1.09, and 1.24 eV, respectively, has been reported.[21] Larger E_b values of 2.2 eV were calculated for the $Au_3/CeO_2(111)$ system[3,20] when nE(Au) was used as a reference. An adsorbed Au_3 moiety represented an isosceles triangle with two Au–Au edges at 2.61 Å and an Au–Au side interacting with the ceria support elongated to 2.76 Å. Indeed, vertical moieties **3a** and **3b** were positively charged: +0.289e and +0.325e, respectively. Similar to Au_2 model **2a**, the Au atoms of Au_3 with no Au–O contact had a negative charge of about –0.1e. Structure **3c** (Table S2) with a linear Au_3 moiety was significantly, by 2.33 eV, less stable (E_b = 0.35 eV). It had three slightly longer Au–O bonds of 2.06–2.10 Å. The Au–Au bonds (2.85–2.88 Å) were sizably longer than those in gas-phase Au_3 species (2.56 Å). Linear model **3c** featured a more positive charge of +0.469e, which reflected stronger oxidation of gold clusters and appearance of two Ce^{3+} ions *vs.* one reduced cerium ion in vertical models **3a** and **3b**. Several attempts to locate a structure with Au_3 moieties lying parallel to the ceria surface were unsuccessful, in line with published data.[4,21]

Tetrameric Au_4 species anchored at O_4 pockets of ceria models with 3D tetrahedral and 2D rhombus shapes, respectively, have been located. The Au_4 tetrahedron was connected with ceria *via* three Au–O bonds of 2.03–2.05 Å (models **4a** and **4b**). The binding energy of Au_4 (0.66 eV) was close to the value for an even-numbered Au_2 moiety. The identical energy was calculated for an $Au_4/CeO_2(111)$ model with a high concentration of Au_4 tetrahedrons per unit cell.[22] Two times larger energy of 1.4 eV was obtained for adsorption of Au_4 at the $CeO_2(111)$ surface with lower density.[4] The values of 2.2 eV were calculated for $Au_4/CeO_2(111)$ models with the use of nE(Au) as a reference.[3,20] The charge of the Au_4 moiety was +0.714e, which supposed deep oxidation reflected in the presence of two Ce^{3+} ions. Moreover, transformation of a 2D Au_4 moiety more stable in a gas phase to a 3D tetrahedron upon adsorption at a ceria support also reflected sizable charge transfer from Au_4 to ceria. Two structures with 2D Au_4 moieties oriented vertically and

horizontally were located. The Au_4 species with a vertical orientation (**4c**) had two Au–O contacts of 2.06 Å and Au–Au distances similar to those in **4a** and **4b** models (Table 1). In line with trimeric **3a** and **3b** structures, the Au_4 moiety charge in model **4c** was small (+0.27e) and consistent with appearance of only one Ce^{3+} center. The 2D Au_4 moiety parallel to the oxide surface (**4d** in Table 1) was coordinated to the ceria surface *via* four slightly elongated Au–O contacts of 2.09–2.15 Å. It featured Au–Au distances of 2.71–2.73 Å, similar to those in a gas-phase Au_4 rhombus.[22] Similar to a 3D structure, this model was characterized by two reduced Ce^{3+} ions despite a smaller cluster charge of +0.48e. Binding energies of flat Au_4 moieties were 0.38 and 0.51 eV, respectively, that is, smaller than that for tetrahedral species. Thus, the shapes and relative energies of ceria-supported $Au_4/Ce_{21}O_{42}$ models were the same as those located on extended $CeO_2(111)$ surfaces.[3]

Summarizing, our calculations revealed that a gold atom, dimer, trimer, and tetramer were bound with O_4 sites of the $CeO_2(100)$ nanofacet with binding energies ranging from 0.66 eV for even-numbered Au_2 and Au_4 species to 1.1 eV for odd-numbered Au_3 moieties with a maximum value of 2.3 eV for a single Au atom. Thus, the binding energy had a nonmonotonous, zigzag-like trend observed earlier[4] for the $Au_n/CeO_2(111)$ systems with small Au_n species at n = 1–4. All clusters, except digold species, featured oxidation with the appearance of reduced Ce^{3+} ions in the vicinity of adsorbed gold species. In line with previous calculations,[3,4,20] the oxidation of Au_3 and Au_4 moieties to +1 and +2 states, respectively, was observed. The two oxidation states +1 and +3 were found to be nearly equally possible for single Au atoms. The latter state was not previously calculated for two-coordinated extraframework Au atoms supported at extended ceria surfaces but the presence of Au^{3+} ions was modeled for four-coordinated intraframework Au ions substituting for Ce ions in a ceria lattice.[23] Deeper oxidation of single Au species observed in this study can be explained by the specific structure of the (100) nanofacet supplying four oxygen atoms located in a plane (the O_4 site). Such isolated Au^{3+} species have been experimentally detected on TiO_2 and CeO_2 surfaces by IR, XAFS, and electron microscopy techniques.[24,25] These sites coexisted with Au^+ and Au^0 sites at temperatures below 0 °C and participated in CO oxidation, but disappeared with increasing temperature and during CO oxidation. Earlier,[12] it has been shown that this O_4 site was adopted for the selective trapping of other 11 single metal atoms as part of the larger ceria nanoparticles $Ce_{40}O_{80}$ and $Ce_{80}O_{160}$.

In general, comparing the bonding of Au_n (n = 1–4) at O_4 site of the (100) nanofacet with that at other ceria surfaces, we can conclude that the bonding of Au_n species with $n > 2$ had similar features (binding energies, numbers of Au–O bonds, cluster charges, and numbers of reduced Ce^{3+} ions) with those for extended CeO_2 surfaces. The binding energy of single Au atoms at the (100) nanofacet was close to that for more reactive extended $CeO_2(110)$ and $CeO_2(100)$ surfaces, but the coordination mode and oxidation state were different. This finding can be crucial for understanding the catalytic properties of single gold atoms highly dispersed at a ceria support.

This research was supported by the Russian Science Foundation (grant no. 25-23-20124, https://rscf.ru/project/25-23-20124/) and a grant of the Krasnoyarsk Regional Science Foundation. The authors thank the Supercomputing Center of the Institute of Computational Modeling, SB RAS (Krasnoyarsk) and Irkutsk Supercomputer Center of SB RAS (HPC-cluster 'Akademik V. M. Matrosov', ISDCT SB RAS; http://hpc.icc.ru) for provided computational resources.

Online Supplementary Materials

Supplementary data associated with this article can be found in the online version at doi: 10.71267/mencom.8141.

References

1 S. Tosoni, *ChemCatChem*, 2019, **11**, 73; https://doi.org/10.1002/cctc.201801082.
2 M. M. Branda, N. C. Hernandez, J. F. Sanz and F. Illas, *J. Phys. Chem. C*, 2010, **114**, 1934; https://doi.org/10.1021/jp910782r.
3 B.-T. Teng, F.-M. Wu, W.-X. Huang, X.-D. Wen, L.-H. Zhao and M.-F. Luo, *ChemPhysChem*, 2012, **13**, 1261; https://doi.org/10.1002/cphc.201101007.
4 J. Engel, S. Francis and A. Roldan, *Phys. Chem. Chem. Phys.*, 2019, **21**, 19011; https://doi.org/10.1039/c9cp03066b.
5 M. Nolan, *J. Chem. Phys*., 2012, **136**, 134703; https://doi.org/10.1063/1.3697485.
6 L. Cui, Y. Tang, H. Zhang, L. G. Hector, Jr., C. Ouyang, S. Shi, H. Li and L. Chen, *Phys. Chem. Chem. Phys*., 2012, **14**, 1923; https://doi.org/10.1039/C2CP22720G.
7 W. Song and E. J. M. Hensen, *J. Phys. Chem. C*, 2013, **117**, 7721; https://doi.org/10.1021/jp400977m.
8 L.-J. Chen, Y. Tang, L. Cui, C. Ouyang and S. Shi, *J. Power Sources*, 2013, **234**, 69; http://doi.org/10.1016/j.jpowsour.2013.01.121.
9 J. Guzman, S. Carrettin, J. C. Fierro-Gonzalez, Y. Hao, B. C. Gates and A. Corma, *Angew. Chem., Int. Ed.*, 2005, **44**, 4778; https://doi.org/10.1002/anie.200500659.
10 A. Migani, G. N. Vayssilov, S. T. Bromley, F. Illas and K. M. Neyman, *Chem. Commun.*, 2010, **46**, 5936; https://doi.org/10.1039/C0CC01091J.
11 A. Migani, G. N. Vayssilov, S. T. Bromley, F. Illas and K. M. Neyman, *J. Mater. Chem.*, 2010, **20**, 10535; https://doi.org/10.1039/C0JM01908A.
12 A. Figueroba, G. Kovács, A. Bruix and K. M. Neyman, *Catal. Sci. Technol.*, 2016, **6**, 6806; https://doi.org/10.1039/C6CY00294C.
13 V. A. Nasluzov, E. A. Ivanova-Shor, A. M. Shor and K. M. Neyman, *Surf. Sci.*, 2019, **681**, 38; https://doi.org/10.1016/j.susc.2018.11.002.
14 G. Kresse and J. Furthmüller, *Phys. Rev. B*, 1996, **54**, 11169; https://doi.org/10.1103/PhysRevB.54.11169.
15 V. A. Nasluzov, E. A. Ivanova-Shor, A. M. Shor, S. S. Laletina and K. M. Neyman, *Materials*, 2021, **14**, 6888; https://doi.org/10.3390/ma14226888.
16 G. Kresse and D. Joubert, *Phys. Rev. B*, 1999, **59**, 1758; https://doi.org/10.1103/PhysRevB.59.1758.
17 G. Kresse and J. Hafner, *Phys. Rev. B,* 1993, **47**, 558; https://doi.org/10.1103/PhysRevB.47.558.
18 A. Chutia, D. J. Willock and C. R. A. Catlow, *Faraday Discuss.*, 2018, **208**, 123; https://doi.org/10.1039/c8fd00002f.
19 C. Zhang, A. Michaelides, D. A. King and S. J. Jenkins, *J. Chem. Phys.*, 2008, **129**, 194708; https://doi.org/10.1063/1.3009629.
20 P. Ghosh, M. F. Camellone and S. Fabris, *J. Phys. Chem. Lett.*, 2013, **4**, 2256; https://doi.org/10.1021/jz4009079.
21 W.-J. Zhu, J. Zhang, X.-Q. Gong and G. Lu, *Catal. Today*, 2011, **165**, 19; https://doi.org/10.1016/j.cattod.2010.11.085.
22 M. J. Piotrowski, P. Tereshchuk and J. L. F. Da Silva, *J. Phys. Chem. C*, 2014, **118**, 21438; https://doi.org/10.1021/jp505216y.
23 Y.-Q. Su, L. Zhang, V. Muravev and E. J. M. Hensen, *Chin. J. Catal.*, 2020, **41**, 977; https://doi.org/10.1016/S1872-2067(19)63468-6.
24 W. Grünert, D. Großmann, H. Noei, M.-M. Pohl, I. Sinev, A. de Toni, Y. Wang and M. Muhler, *Angew. Chem., Int. Ed.*, 2014, **53**, 3245; https://doi.org/10.1002/anie.201308206.
25 M. Han, X. Wang, Y. Shen, Ch. Tang, G. Li and R. L. Smith, Jr., *J. Phys. Chem. C*, 2010, **114**, 793; https://doi.org/10.1021/jp908313t.

Received: 7th July 2026; Com. 26/8141

Mendeleev Commun., 2027, **37**, in press

Contents entry

Bonding of Au_n (n = 1–4) gold species at the $Ce_{21}O_{42}$ ceria nanoparticle

Elena A. Ivanova-Shor, Aleksey M. Shor, Svetlana S. Laletina, Vladimir A. Nasluzov

